THE JOURNAL OF PHYSICAL CHEMISTRY B

pubs.acs.org/JPCB Article

Time-Resolved Fluorescence and Essential Dynamics Study on the Structural Heterogeneity of p53DBD Bound to the Anticancer p28 Peptide

Anna Rita Bizzarri* and Salvatore Cannistraro

Cite This: https://dx.doi.org/10.1021/acs.jpcb.0c06778 Read Online

ACCESS | Metrics & More | Article Recommendations

ABSTRACT: Time-resolved fluorescence emission was combined with molecular dynamics (MD) simulations to investigate the DNA-binding domain (DBD) of the tumor suppressor p53 alone and its complex with the anticancer peptide p28 (DBD/p28). The fluorescence emission decay of the lone Trp residue, from both DBD and DBD/p28, was well-described by a stretched exponential function. Such a behavior was ascribed to heterogeneity in the Trp relaxation behavior, likely due to the coexistence of different conformational states. The increase of the stretching parameter, on passing from DBD to DBD/p28, indicates a reduced heterogeneity in the Trp146 environment for DBD/p28. Moreover, the effects of p28 on the global dynamics of DBD were analyzed by the essential dynamics method on 30 ns long MD trajectories of both DBD and DBD/p28. We found the establishment of wide-amplitude anharmonic modes throughout the DBD molecule, with a particularly high amplitude being detected in the DNA-binding region. These modes are significantly reduced when DBD is bound to p28, consistently with a structure stabilization. In summary, the results indicate that p28 binding has a strong effect on both the local and global heterogeneity of DBD, thus providing some hints to the understanding of its anticancer activity.

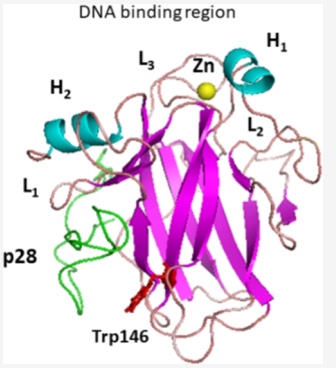

INTRODUCTION

It is now well ascertained that the structure−function paradigm, central in the biology of proteins, is to be extended to include intrinsically disordered proteins (IDPs), which possess (a few or many) intrinsically disordered regions.[1] IDPs are present in living organisms with a higher frequency as far as the complexity level of organisms increases.[2] The partial lack of a well-defined structure confers to these proteins some advantages in terms of functionality. Indeed, thanks to the coexistence in solution of several widely different conformations, IDPs acquire the capability to bind different biological molecules (proteins, DNA, and RNA), by constituting then a sort of hub with a crucial role in many biological processes.[2,3]

The tumor suppressor p53 is a very important IDP and is at the center of a complex interaction network regulating numerous cellular processes, such as cell cycle progression, apoptosis induction, and DNA repair.[4,5] Under physiological conditions, p53 possesses both structured and disordered domains.[6] More specifically, p53 is a tetrameric protein composed of four identical subunits, with each monomer consisting of an N-terminal transactivation domain (NTD), a C-terminal domain (CTD), and a core domain, with large structured regions, which binds DNA (DBD).[7−10] Since the oncosuppressive function of p53 is reduced or inactivated in many human cancers, large efforts are devoted to identify, design, and potentiate molecules able to stabilize or restore the anticancer activity of p53, with particular attention to its DBD, which is incidentally mutated in more than half of the human cancers.[11−13]

We have investigated the interaction between full-length p53, or its isolated domains (DBD or even NTD), and the blue-copper-containing protein Azurin (from *Pseudomonas aeruginosa* bacterium), which has been found to preferentially enter cancer cells and form a specific and stable complex with p53, with a concomitant increase of its tumor suppressor activity.[14−19] More recently, we have focused our attention on the p28 peptide, which is formed by the α-helix fragment (50−77 AA) of Azurin and is endowed with an efficient cellular penetration ability. Upon entering the cell, p28 can bind to p53, leading to an increase of its intracellular levels. Indeed, p28 inherits the overall tumoricidal activity of Azurin but with lesser side effects.[20] The interaction between the p28 peptide and DBD has been investigated by atomic force spectroscopy (AFS), surface plasmon resonance (SPR), Raman, fluorescence, and Förster resonance energy transfer (FRET) techniques; in the last case, DBD containing a lone tryptophan residue (Trp146) has been used. These studies have allowed us

Received: July 24, 2020
Revised: October 14, 2020

to demonstrate the formation of a stable complex between DBD and p28 and evaluate the corresponding binding affinity. Additionally, the distance between the donor (the lone Trp146 residue) and the acceptor (a suitable dye bound to the N-terminal of p28) has been estimated. Knowledge of this distance combined with the results from a docking study, refined by molecular dynamics (MD) simulations, has allowed us to single out the best model for the DBD-p28 complex.[21]

In this context, it would be interesting to investigate the structural and dynamical effects that are induced by the binding of p28 to DBD. To address these aspects, we have applied time-resolved fluorescence combined with molecular dynamics (MD) simulations on both DBD and its complex with the p28 peptide (DBD/p28). We found that the time-resolved fluorescence emission of the lone Trp146 of DBD is characterized by a stretched exponential decay, indicative of a heterogeneous relaxation mechanism of the Trp residue. Such a result has been put into relationship to the coexistence, in solution, of different conformational states, which can be ascribed to the partial disorder character of DBD. The conformational heterogeneity around Trp146 has been observed to persist in DBD bound to p28, but to a lower extent, with this being indicative of a fine tuning of the structural disorder of DBD as induced by binding of p28. To elucidate the p28 effects on the global dynamics of DBD, we have carried out MD simulations on DBD and DBD/p28, within the same temporal window of the fluorescence experiments. Essential dynamics (ED) analysis of the corresponding MD trajectories has put into evidence the existence of wide anharmonic modes within the DBD molecule. The amplitudes of these modes undergo a significant reduction when DBD is bound to p28. All these results, consistent with the intrinsically disordered character of the biomolecule, could be of some help for the biophysical interpretation of the anticancer role of p28, as exerted upon its interaction with DBD.

EXPERIMENTAL AND COMPUTATIONAL METHODS

Materials. Recombinant human DNA-binding domain (DBD) of p53 (residues 94−300) (23400 Da, purity > 90%, verified by high-performance liquid chromatography (HPLC) and MS by the producer), containing a lone tryptophan (Trp146), was purchased from Genscript (Piscataway, NJ) using the BacPower Guaranteed Bacterial Protein Expression Service.

The p28 peptide (LSTAADMQGVVTDGMASGLDK-DYLKPDD, 2914 Da) was synthesized and verified by MS and HPLC (93% purity) by GenScript (Piscataway, NJ). Human serum albumin (HSA) from human serum lyophilized powder, essentially globulin free with a purity degree higher than 99%, was purchased from Sigma Aldrich and used without further purification. Phosphate-buffered saline (PBS, 50mM at pH 7.4) was used as buffer.

Absorbance, Static, and Time-Resolved Fluorescence Measurements. Absorbance spectra were recorded at room temperature by a double-beam Jasco V-550UV/visible spectrophotometer using 1 cm path length cuvettes and 1 nm bandwidth in the spectral region 220−750 nm; PBS was used as reference.

Steady-state fluorescence measurements were performed with a FluoroMax-4 spectrofluorometer (Horiba Scientific, Jobin Yvon, France). The samples were excited at 295 nm and fluorescence emission was collected from 305 to 580 nm using 1 nm increments and an integration time of 0.50 s. A 2 nm bandpass was used in both excitation and emission paths. Spectra were acquired in the signal to reference (S/R) mode to take into account for random lamp intensity fluctuations. Emission spectra were corrected for Raman contribution from the PBS.

Time-resolved fluorescence measurements were performed at room temperature with the time-correlated single photon counting method using the abovementioned FluoroMax-4 spectrofluorometer, operating at a repetition rate of 1 MHz and running in reverse mode. The apparatus was equipped with a pulsed nanosecond light-emitting diode (LED) excitation head (Horiba Scientific, Jobin Yvon), emitting at 295 nm with a bandwidth of 20 nm (which was lowered to 4 nm by the slits) and a temporal width lower than 1 ns. Fluorescence lifetime data were detected at 345 nm and acquired until the peak signal reached 10k counts and were analyzed using the impulse response function (DAS6 software, Horiba Scientific). For each fluorescence experiment, 10 measurements were performed on independently prepared samples by determining the average and the corresponding standard deviation.

Analysis of Time-Resolved Fluorescence. Fluorescence decays were preliminarily analyzed by the sum of exponential components by employing a non-linear least square analysis including deconvolution of the prompt from Horiba, Jobin Yvon

$$I(t) = a_0 + \sum_{i=1}^{n} a_i e^{(-t/\tau_i)} \quad (1)$$

where $I(t)$ is the time-dependent intensity, a_0 gives the background, and a_i are pre-exponential factors representing fractional contribution to the time-resolved decay of the ith component with lifetime τ_i. The goodness of the fit was judged in terms of both the χ^2 value and weighted residuals. The average fluorescence lifetime $\langle\tau\rangle$ was then calculated by

$$\langle\tau\rangle = \frac{\sum_{i=1}^{n} a_i\tau_i}{\sum_{i=1}^{n} a_i} \quad (2)$$

Modeling Procedures. The structure of DBD was derived from the B chain of DBD in complex with a consensus DNA (1TUP entry from the protein data bank).[10] The structure was suitably adjusted to match the DBD portion used in fluorescence and FRET experiments. In particular, the short 290−300 AA portion was added using the I-TASSER suite.[22] The structure of DBD is composed of two antiparallel β-sheets of four and five strands, respectively, forming a β-sandwich structure (see Figure 1). The Zn ion is tetrahedrically coordinated to the side chains of Cys176, His179, Cys238, and Cys242, forming a Zn-finger motif, which is connected to the L_2 and L_3 loops.[23] The interaction of the Zn ion with its ligands was treated through a bonded approach, in which the Zn−N and Zn−S bonds and S−Zn−S angles were set according to the parameters provided in refs 21, 24−26. The binding of DBD to DNA occurs within the H_2 and the L_1 and L_3 loops in a region, conventionally chosen to be the northern part of the molecule.

The initial coordinates of the DBD-p28 complex were taken from the "best model" as obtained by a previous study based on a computational docking approach exploiting the structural

https://dx.doi.org/10.1021/acs.jpcb.0c06778
J. Phys. Chem. B XXXX, XXX, XXX−XXX

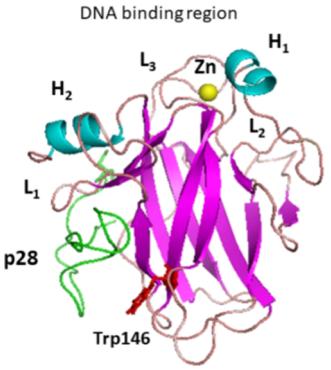

Figure 1. Structure of the complex between DBD (magenta) and p28 (green), according to the "best model" obtained by the method reported in ref21; the Zn ion is represented by a yellow sphere and Trp146 in blue.

information derived from FRET data,[21] with such a model being shown in Figure 1.

Molecular Dynamics (MD) Simulations and Analysis. MD simulations of DBD and the DBD-p28 complex in water were carried out by the GROMACS 2018 package[27] using AMBER03 Force Field DBD and p28[28] and SPC/E for water.[29] DBD and DBD-p28 were centered in a cubic box of edge 9.0 nm. Simulations were performed by following the procedures described in refs 21, 30. Briefly, the boxes were filled with water molecules to reach a hydration level of 9 g water/g protein. The ionization states of protein residues were fixed at pH 7, and Cl− ions (one for DBD and five for DBD/p28) were added to keep the systems electrically neutral. H bonds were constrained with the LINCS algorithm,[31] while the particle mesh Ewald (PME) method[32,33] was used to calculate the electrostatic interactions with a lattice constant of 0.12 nm. Periodic boundary conditions in the NPT ensemble with T = 300 K and p = 1 bar with a time step of 1 fs were used. The temperature was controlled by the Nosé−Hoover thermostat with a coupling time constant τ_T of 0.1 ps,[34] while Parrinello−Rahman extended ensemble, with a time constant t_P of 2.0 ps, was used to control the pressure.[35] Each system was minimized and then heated to 300 K with steps at 50, 100, 150, and 250 K. MD trajectories were analyzed by the GROMACS package tools.[27] Each model was submitted to a 30 ns long MD trajectory, replicated 10 times. The temporal evolution of the systems was monitored by following the root mean square displacement (RMSD), root mean square fluctuations (RMSF), surface accessible surface (SAS) area, and the methods described in ref36. The equilibration of each system was checked by analyzing the RMSD as a function of time. The figures were created with Pymol and VMD.[37,38]

Essential Dynamics (ED) Analysis. The sampled MD trajectories were analyzed by ED, a method based on principal component analysis (PCA) aimed at identifying a new reference frame to describe the overall dynamics of the system and then allowing to extract the protein motions mostly contributing to the overall dynamics.[39] ED was carried out by the Covar and Anaeig subroutines of GROMACS.[40,41] After a least-square fit to remove roto-translations, the covariance matrix C_{ij} was calculated by

$$C_{ij} = \langle (x_i - \langle x_i \rangle)(x_j - \langle x_j \rangle) \rangle \quad (3)$$

where x_i are the x, y, and z Cartesian coordinates of the C_α atoms of DBD and $\langle\rangle$ indicates the average over the trajectories. C_{ij} was diagonalized by finding out a set of eigenvalues and eigenvectors; the eigenvectors correspond to directions in an N-dimensional space and are called principal coordinates (PCs), while the eigenvalues represent the total mean square fluctuation along the corresponding eigenvectors.

RESULTS AND DISCUSSION

Fluorescence Emission. Figure 2A shows the emission spectrum of DBD (black line) and DBD after the addition of p28 (DBD/p28; red line) in a 1:1 molar ratio. Both spectra have been obtained by excitation at 295 nm, at which the lone tryptophan residue (Trp146) from DBD still absorbs, while the Tyr and Phe residues, from DBD and p28, are not substantially excited.

The spectrum of DBD is peaked at about 345 nm (see the arrow), pointing out that Trp146 is almost fully exposed to the solvent, this being consistent with the SAS for Trp146 of about 0.8 nm^2, as evaluated from the DBD X-ray structure.[42] The fluorescence emission intensity of DBD/p28 is reduced with respect to that of DBD, although no significant wavelength shift of the peak is observed. In particular, we found (32 ± 2) × 10^3 counts for DBD and (25 ± 2) × 10^3 counts for DBD/p28, by averaging the results over 10 samples. Such a 20% decrease in the fluorescence intensity indicates that p28 affects the fluorescence emission of DBD without changing the solvent exposition of Trp146. This result finds a correspondence with the formation of a stable complex between DBD and p28, in which Trp146 is not directly involved, as previously found.[21] Indeed, we recall that static fluorescence experiments demonstrated the formation of a stable complex between DBD

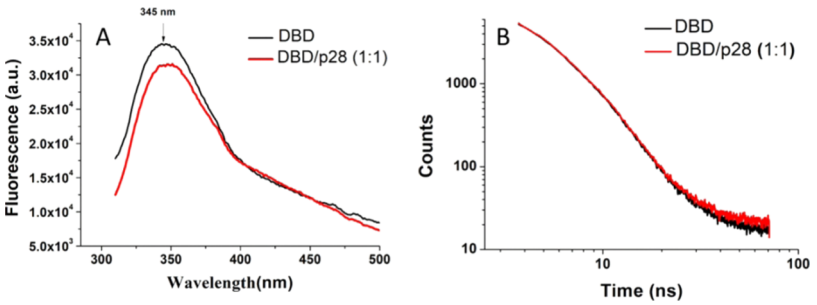

Figure 2. (A) Fluorescence emission spectra of DBD (black line) and DBD in the presence of p28 (1:1) (red line), registered upon excitation at 295 nm, and corrected for the Raman scattering of the buffer. (B) Time-resolved fluorescence emission of DBD (black line) and DBD in the presence of p28 (1:1) (red line). The decays have been obtained by exciting the samples with a 295 nm nanoLED pulse, while emission was collected at 345 nm.

https://dx.doi.org/10.1021/acs.jpcb.0c06778
J. Phys. Chem. B XXXX, XXX, XXX−XXX

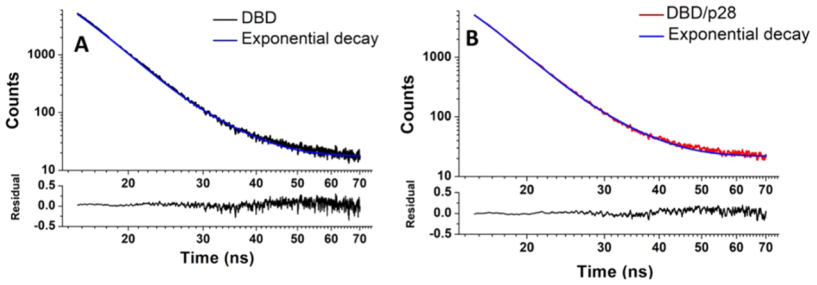

Figure 3. Fits (blue curves) by the sum of two exponential decays through eq 1 of fluorescence emission data for (A) DBD (black curve) and (B) DBD/p28 (red curve); the fitting parameters are reported in Table 1.

Table 1. Fitting Parameters of Time-Resolved Fluorescence Emission Data for DBD and DBD/p28, as Obtained by Averaging the Results over 10 Curves, by the Sum of Two Exponentials through eq 1

sample	τ_1 (ns)	τ_2 (ns)	$\langle\tau\rangle$ (ns) (eq 2)	a_1	a_2	χ^2 range
DBD	2.63 ± 0.03	7.32 ± 0.03	3.24 ± 0.03	36.3 ± 0.1	5.5 ± 0.1	1.1−1.2
DBD/p28	2.63 ± 0.03	7.34 ± 0.03	3.21 ± 0.03	35.5 ± 0.1	5.3 ± 0.1	1.1−1.2

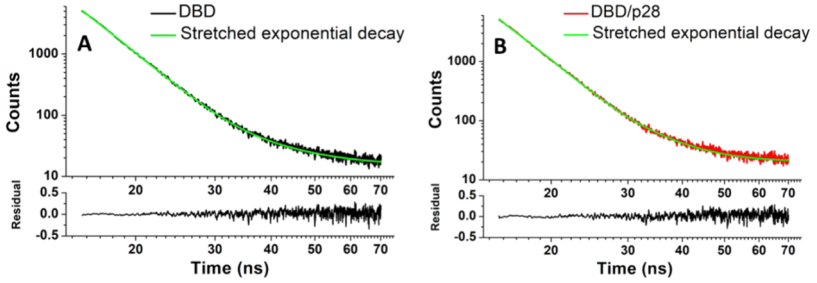

Figure 4. Fits (green curves) by the sum of a simple exponential decay and a stretched exponential decay through eq 4 of fluorescence emission data for: (A) DBD (black curve) and (B) DBD/p28 (red curve); the fitting parameters are reported in Table 1.

Table 2. Fitting Parameters of Time-Resolved Fluorescence Emission Data for DBD and DBD/p28, as Obtained by Averaging the Results from 10 Curves, by the Sum of an Exponential and a Stretched Exponential through eq 4

sample	τ_1 (ns)	τ_2 (ns)	β	a_1	a_2	χ^2 range
DBD	2.63 ± 0.04	3.56 ± 0.03	0.74 ± 0.01	2.4 ± 0.1	2.4 ± 0.1	1.0−1.1
DBD/p28	2.63 ± 0.03	3.55 ± 0.03	0.82 ± 0.01	2.4 ± 0.1	2.4 ± 0.1	1.0-1.1

and p28 with a dissociation constant K_D of ∼ 7.4 × 10^{-6} M.[21] Figure 2B representatively shows the time-resolved fluorescence emissions of DBD (black line) and DBD/p28 (red line), excited at 295 nm by a nanosecond pulsed LED. The two fluorescence decays appear practically identical at times shorter than 30 ns, while they differ more than 10% at longer times.

At first, the emission data of both DBD and DBD/p28 have been fitted by the sum of two exponential decays using eq 1. Although a satisfactory description of the global decay for both the samples has been obtained for shorter decay times, a slight deviation between experimental and fitted curves is detected at longer times (see an example in Figure 3A,B). The fitting parameters, extracted by eq 1, and averaged from a collection of 10 independently prepared samples, are reported in Table 1. The resulting lifetimes are practically the same for both the samples, and they are in agreement with the values previously obtained ((3.19 ± 0.01) and (3.17 ± 0.02) ns), for DBD and DBD/p28, respectively.[21,43] We also note that the amplitudes of the two pre-exponential factors are very similar for the two samples, thus indicating that the binding of p28 does not modify the decay populations in DBD.

To more precisely describe the time-resolved fluorescence emission, and by taking into consideration the disordered character of DBD, we were led to consider the possibility of a stretched exponential decay, commonly used to describe the fluorescence emission of heterogeneous systems, for both the fast and slow decay components.[44] We found that the fluorescence emission intensity of the DBD and DBD/p28 samples can be well fitted by the sum of a simple exponential decay for the fast component and a stretched exponential decay for the slow one. This could be justified by the reported evidence that protein motions are characterized by an almost homogeneous behavior, while the slower one is almost heterogeneous, reflecting collective motions.[45] In particular, the following expression has been used

$$I(t) = a_0 + a_1 e^{(-t/\tau_1)} + a_2 e^{(-t/\tau_2)\beta} \quad (4)$$

where a_0 describes the background, a_1 and a_2 are the pre-exponential factors for the simple and stretched exponential decays, respectively, τ_1 and τ_2 are the corresponding lifetimes, and β is the stretching parameter, which should fall between 0 and 1, with the stretching character being progressively more relevant as far as it becomes less than 1.

Representative fits of the experimental time-resolved fluorescence emission using eq 4 are shown in Figure 4. At visual inspection, the agreement between fitted curves and

https://dx.doi.org/10.1021/acs.jpcb.0c06778
J. Phys. Chem. B XXXX, XXX, XXX−XXX

experimental data is very good throughout the time range and it is significantly improved in comparison to that obtained using two exponentials (see the residual plots in Figures 3 and 4) and witnessed by the lower chi-square values (see Tables 1 and 2). The fitting parameters, averaged from a collection of 10 independently prepared samples, are reported in Table 2. The fast component, following a simple exponential decay, is characterized by the same decay time for both the samples, such a time being also equal to that emerging from the fit with two exponential decays. Also, in this case, the amplitudes of the two pre-exponential factors are substantially the same for the two samples. The stretched exponential decay is characterized by almost the same decay times for DBD and DBD/p28, with the β parameter significantly deviating from 1 for both the samples. However, β is slightly lower for DBD (β = 0.74) compared to DBD/p28 (β = 0.82).

A stretched exponential decay, with a β parameter lower than 1, generally reflects a glass-like character of the system, and it has been observed in many disordered systems, including biomolecules.[46] In proteins, a stretched exponential function has been used to describe different processes, such as photodissociation, protein, and hydration water dynamics, and it has been put into relationship to the sampling of dynamical states differing among them for structural details (usually called conformational substates).[45,47,48] The emission fluorescence decay of Trp residues in proteins has been fitted by a stretched exponential and interpreted in terms of a heterogeneous environment around Trp residues, which may include contributions from both the protein matrix and the solvent.[44,49,50] For single-tryptophan proteins, as in our case, the observation of a stretched exponential for the emission fluorescence decay of Trp could be directly related to the behavior of a well-defined region of the protein rather than to the complexity arising from the superposition of different contributions. In this respect, for comparison, we have also analyzed the time-resolved fluorescence emission decay of the HSA protein, which contains a lone Trp (Trp214) exposed to the solvent, with an SAS value of about 0.7 nm^2, as evaluated from the X-ray structure.[51]

Figure 5 shows the time-resolved fluorescence emission data of HSA (black curve) excited at 295 nm by a nanoLED pulse; the corresponding fit using the sum of two exponential decay (red curve) is also shown. The fit almost perfectly describes the data and the resulting average lifetime of (5.43 ± 0.08) ns, which is in very good agreement with the literature (including our previous results).[52,53] The fit by the sum of exponentials for HSA supports the hypothesis that the appearance of a stretched exponential decay in DBD and DBD/p28 can be ascribed to some heterogeneity in the Trp146 environment arising from the protein matrix. In other words, the observation of a stretched exponential decay in DBD can be put into relationship to a local structural disorder of the protein, as monitored by Trp146. On such a basis, the slight increase of the β exponent observed for the Trp146 emission of DBD/p28 with respect to DBD indicates a decrease in the structural disorder of DBD upon its binding to p28. In summary, the time-resolved fluorescence emission decay of Trp146 in DBD, alone and bound to p28, shows a heterogeneous relaxation behavior, which reflects a local disorder undergoing a decrease when DBD is bound to p28. Furthermore, since the p28 binding is not directly involved with Trp, as previously demonstrated,[21] these results suggest that p28 can affect the global dynamics of DBD.

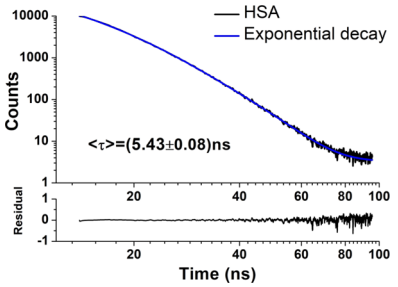

Figure 5. Fluorescence decay (black lines) obtained by exciting with a 295 nm nanoLED pulse; emission was collected at 345 nm. The blue line is a fit by the sum of two exponential decays. The average lifetime, as evaluated by eq 2, is reported.

MD simulation results. To closely investigate the effects induced by p28 on both the whole structure of DBD and the Trp146 environment, we have performed MD simulations on both DBD alone and the DBD/p28 complex. For each system, we have collected MD simulation runs of 30 ns; such a time interval is comparable with the temporal windows of the fluorescence emission. For the DBD/p28 complex, whose structure is not known, we have used the model previously derived from FRET data (see the section Experimental and Computational Methods and ref21).

First, we have assessed the stability of the complex by monitoring the distance between DBD Trp146 and the p28 Leu19 residue, the latter one being the p28 residue closest to DBD. Figure 6A shows the trend of this distance as a function of time. For all of the runs, we noted that the distance varies in time between 0.8 and 1.0 nm. These results indicate that p28 remains in the close proximity of DBD during the run, and then they support the stability of the DBD/p28 complex.

Figure 6B shows a representative temporal evolution of the RMSDs, averaged over all atoms, for DBD alone (black curve) and for DBD/p28 (red curve). In both cases, the RMSDs rapidly increase by reaching a plateau at about 0.25 nm within 2 ns, consistently with a quick relaxation of the structure. Successively, we note an almost constant regime, in which fast fluctuations are superimposed on slower ones. To avoid instabilities due to protein equilibration, we have discarded the first 3 ns, and the successive 27 ns long time intervals have been then taken into consideration for further analysis.

Figure 7A,B shows the time-averaged RMSDs and RMSFs, respectively, as a function of the residue number of DBD alone (black lines) and of DBD/p28 (red lines), the secondary structure being sketched at the bottom. RMSDs and RMSFs exhibit similar profiles with almost all of the peaks located at the same positions along the protein chain. Similar trends have been observed for the other runs. The largest part of the peaks appears in correspondence of the turns and bends, consistently with the higher flexibility of these regions. The RMSDs in the region involved in the binding with p28, marked with blue stars in Figure 7, show slightly larger deviations from the initial structure, consistent with a rearrangement of the DBD structure upon binding the p28. At the same time, a reduction in the RMSF values occurs, with this reflecting a decreased mobility of residues in close contact with the peptide. Additionally, for the region around Trp146 (marked with circles in Figure 7), the RMSDs show both increase and decrease on passing from DBD to DBD/p28, consistent with slight structural changes of the Trp146 environment. At the

https://dx.doi.org/10.1021/acs.jpcb.0c06778
J. Phys. Chem. B XXXX, XXX, XXX−XXX

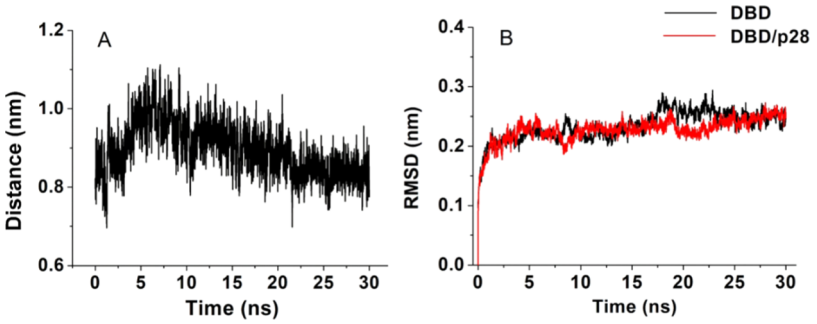

Figure 6. (A) Distance between Trp146 (DBD) and Leu19 (p28) as a function of time. (B) RMSD, averaged over all atoms, as a function of time for DBD alone (black line) and complexed with p28 (red line).

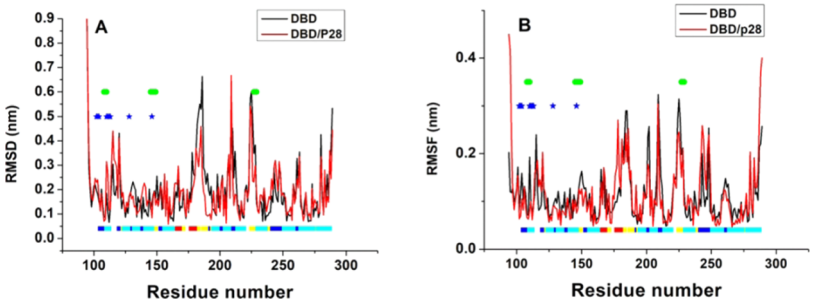

Figure 7. (A) RMSD and (B) RMSF as a function of the residue number for DBD (black lines) and DBD complexed with p28 (red lines). The secondary structure is sketched in the bottom: turn (blue squares), α-helices (red squares), bend (yellow squares), and β-sheets (cyan squares). Blue stars mark the residues involved in the binding with p28, while green circles mark the residues with a distance lower than 0.5 nm from Trp146.

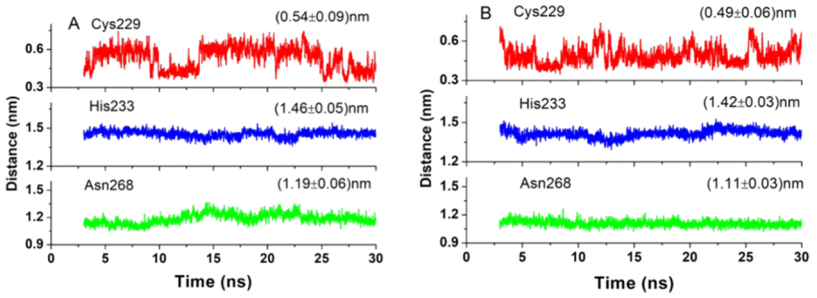

Figure 8. Temporal evolution of the distance between Trp146 and Cys229 (red curves), His233 (blue curves), and Asn268 (green curves) for DBD (A) and DBD/p28 (B).

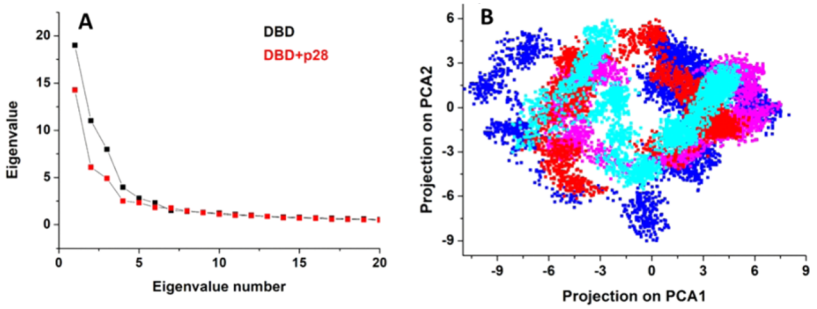

Figure 9. (A) Eigenvalues as a function of the eigenvalue number for DBD and DBD/p28. (B) 2D plot of the projection of PC1 versus the projection of PC2 for DBD (blue and magenta spots) and DBD/p28 (red and cyan spots).

same time, the RMSFs undergo a slight decrease, indicating a lower flexibility for this region when DBD is bound to p28. Then, we more closely analyzed the region around Trp146 to elucidate possible changes affecting the fluorescence properties of DBD. Accordingly, we monitored the distance between Trp146 and the Cys229, His233, and Asn268 residues, all of them being located within 1.5 nm from Trp146 and assumed to be more susceptible to quench the Trp fluorescence.[54] Representative plots for the temporal evolution of these three distances are shown in Figure 8. We note fast fluctuations on which some jumps are superimposed; a higher number of jumps are detected for Cys229, which is the closest residue to

https://dx.doi.org/10.1021/acs.jpcb.0c06778
J. Phys. Chem. B XXXX, XXX, XXX−XXX

Trp146. The average distances and the standard deviations (see Figure 8) are indicative that small changes occur upon binding of p28 to DBD, with this being consistent with a structural rearrangement of the protein region around Trp146. Interestingly, the standard deviations of the analyzed distances are found to be slightly lower on passing from DBD to DBD/p28. Such a finding could be attributed to the reduction of the structural heterogeneity around Trp146, which is in agreement with what has been found by fluorescence.

To get insights into the global dynamics of DBD and DBD/p28, we analyzed their MD trajectories by the ED method, which restricts the conformational space, allowing us to find out the relevant protein motions. The first 20 eigenvalues extracted from the covariance matrix of the atomic fluctuations and ranked in a decrement order, for DBD (black squares) and DBD/p28 (red squares), are shown in Figure 9A. In both cases, the eigenvalues rapidly decrease, reaching an almost stable value (i.e., a value lower than 10% of the maximum) at the eigenvalue no. 8. Similar results have been obtained for other trajectories, in which a stable value is reached for eigenvalues between no. 7 and no. 10. On average, the first 10 eigenvalues capture about 50% of the fluctuations for DBD and about 40% for DBD/p28. Additionally, the first eigenvalue accounts for a slightly higher percentage for DBD (23%) with respect to DBD/p28 (20%). These results indicate that the most relevant motions are concentrated in a few modes, whose dimensionality is represented by the number of eigenvalues accounting for the most relevant modes, with such an effect being more relevant for DBD with respect to DBD/p28.

Figure 9B shows a 2D plot of the projection on the first eigenvalue (PC1) versus the second one (PC2) for the two trajectories of DBD (blue and magenta spots) and DBD/p28 (red and cyan spots); such a plot provides a global description of the configurational space sampled by the system. In all of the cases, the spots cover a rather wide region indicating the establishment of extended collective modes in DBD; these modes can be ascribed to the exploration of different structural conformations. From Figure 9B, we also note that the extension of the plot region is significantly reduced for DBD/p28 in comparison to that of DBD alone. This means that the collective modes of DBD complexed with p28 are characterized by lower amplitudes, and p28 affects the global dynamics of DBD by restringing the explored conformation states.

Figure 10 shows the snapshots of the extreme projections on the first eigenvectors for DBD and DBD/p28, from the same two runs of Figure 9B. From this figure, it is evident that along the first eigenvector, the molecule can assume different arrangements throughout the whole structure, with this supporting the establishment of anharmonic modes. The most marked variability is observed in correspondence of the H_1 and H_2 helices and of almost all turns and bends, while small variability occurs at the β-sheets. Similar results have been obtained for the other runs. Generally, such a behavior finds correspondence with the disordered character of DBD. Indeed, regions characterized by wide anharmonic modes are expected to have higher flexibility, which could also confer an increased capability to bind different ligands. On the other hand, regions providing the skeleton of the molecule, such as the β-sheets, show restricted anharmonic modes. From Figure 10, we also note that the extreme projections on the first eigenvector are significantly reduced for DBD/p28 with respect to DBD (Figure 10C,D), with this being particularly

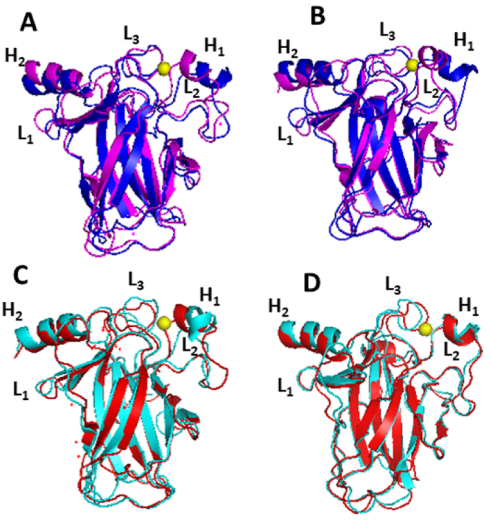

Figure 10. Extreme trajectory conformations projected along the first eigenvector for DBD (A, B) and DBD/p28 (C, D). The Zn ion is represented as a yellow sphere.

evident for the H_1 and H_2 helices, as well as at the turn located at the top of the molecule, which is devoted to the binding of DNA. The observed decrease in the amplitude of anharmonic modes on DBD/p28 can be consistent with the stabilization of the protein, which could also lead to some changes in the binding properties of DBD. In other words, the lower structural heterogeneity occurring in DBD/p28 with respect to DBD could give rise to the modulation of the binding capability of DBD, and it deserves further investigations, even in the perspective of designing new drugs acting on the p53 functionality. Finally, it is interesting to note that the binding of small molecules in a well-defined region of DBD can affect the whole DBD structure, consistent with the complex character of proteins, in which a small change might result in drastic effects in the global system.

In summary, the ED analysis of MD trajectories shows that the binding of p28 to DBD induces global changes in the dynamics of DBD, yielding the reduction of collective motions. These results can also provide a picture to interpret the observed modulation of the heterogeneity around Trp146 when DBD is bound to p28, as emerging from fluorescence emission data. More generally, the reduction of amplitude collective motions could have some implications on the capability of DBD to bind to possible partners through a global reorganization. These aspects should be further investigated even in connection with the possibility of enhancing the anticancer role of p53.

CONCLUSIONS

The analysis of the time-resolved emission fluorescence of the lone Trp146 of DBD, which constitutes the core of the tumor suppressor p53, has put into evidence a stretched exponential decay, indicative of a local heterogeneity around the Trp residue. Such a result can be ascribed to the existence of slightly different protein conformations sampled in the analyzed temporal window and is consistent with the partially disordered character of DBD. The increase of the stretching parameter when DBD is complexed with the anticancer peptide p28 reflects a reduction of the heterogeneity in the Trp146 environment. Such a behavior suggests the capability of p28 to modulate the conformational space explored by

https://dx.doi.org/10.1021/acs.jpcb.0c06778
J. Phys. Chem. B XXXX, XXX, XXX−XXX

DBD. The ED analysis of MD simulated trajectories of DBD alone and of the DBD/p28 complex has shown the establishment of wide collective modes throughout the DBD molecule. The amplitude of these modes is wider for those regions devoted to the ligand binding, such as the DNA-binding domain. The reduction of the mode amplitude in the DBD/p28 complex indicates that the structural heterogeneity of DBD undergoes a marked modulation upon its binding to the p28 peptide. Additionally, a decrease of local heterogeneity around Trp146 has also been observed. These results support the hypothesis that slight local changes of DBD could globally affect the whole DBD dynamics. Additionally, they provide some hints to analyze and improve the role of drugs able to restore or enhance the anticancer capability of p53.

AUTHOR INFORMATION

Corresponding Author

Anna Rita Bizzarri − *Biophysics and Nanoscience Centre, DEB, Università della Tuscia, 01100 Viterbo, Italy;* orcid.org/0000-0003-3298-6639; Phone: +39 0761357031; Email: bizzarri@unitus.it

Author

Salvatore Cannistraro − *Biophysics and Nanoscience Centre, DEB, Università della Tuscia, 01100 Viterbo, Italy*

Complete contact information is available at: https://pubs.acs.org/10.1021/acs.jpcb.0c06778

Notes

The authors declare no competing financial interest.

REFERENCES

(1) Oldfield, C. J.; Dunker, A. K. Intrinsically Disordered Proteins and Intrinsically Disordered Protein Regions. *Annu. Rev. Biochem.* **2014**, *83*, 553−584.

(2) Berlow, R. B.; Dyson, H. J.; Wright, P. E. Functional advantages of dynamic protein disorder. *FEBS Lett.* **2015**, *589*, 2433−2440.

(3) Huang, Y.; Liu, Z. Kinetic advantage of intrinsically disordered proteins in coupled folding-binding process: a critical assessment of the "fly-casting" mechanism. *J. Mol. Biol.* **2009**, *393*, 1143−1159.

(4) Vousden, K. H.; Lane, D. P. p53 in health and disease. *Nat. Rev. Mol. Cell Biol.* **2007**, *8*, 275−283.

(5) Kruiswijk, F.; Labuschagne, C. F.; Vousden, K. H. p53 in survival, death and metabolic health: a lifeguard with a licence to kill. *Nat. Rev. Mol. Cell Biol.* **2015**, *16*, 393−405.

(6) Joerger, A. C.; Fersht, A. R. The tumor suppressor p53: from structures to drug discovery. *Cold Spring Harb. Perspect. Biol.* **2010**, *2*, No. a000919.

(7) Cañadillas, J. M. P.; Tidow, H.; Freund, S. M. V.; Rutherford, T. J.; Ang, H. C.; Fersht, A. R. Solution structure of p53 core domain: structural basis for its instability. *Proc. Natl. Acad. Sci. U.S.A.* **2006**, *103*, 2109−2114.

(8) Pagano, B.; Jama, A.; Martinez, P.; Akanho, E.; Bui, T. T. T.; Drake, A. F.; Fraternali, F.; Nikolova, P. V. Structure and stability insights into tumour suppressor p53 evolutionary related proteins. *PLoS One* **2013**, *8*, No. e76014.

(9) Bell, S.; Klein, C.; Mueller, L.; Hansen, S.; Buchner, J. P53 Contains Large Unstructured Regions in Its Native State. *J. Mol. Biol.* **2002**, *322*, 917−927.

(10) Cho, Y.; Gorina, S.; Jeffrey, P. D.; Pavletich, N. P. Crystal structure of a p53 tumor suppressor-DNA complex: understanding tumorigenic mutations. *Science* **1994**, *265*, 346−355.

(11) Merkel, O.; Taylor, N.; Prutsch, N.; Staber, P. B.; Moriggl, R.; Turner, S. D.; Kenner, L. When the guardian sleeps: Reactivation of the p53 pathway in cancer. *Mutat. Res.* **2017**, *773*, 1−13.

(12) Muller, P. A. J.; Vousden, K. H. Mutant p53 in Cancer: New Functions and Therapeutic Opportunities. *Cancer Cell* **2014**, *25*, 304−317.

(13) Friedler, A.; Hansson, L. O.; Veprintsev, D. B.; Freund, S. M. V.; Rippin, T. M.; Nikolova, P. V.; Proctor, M. R.; Rüdiger, S.; Fersht, A. R.; Rudiger, S.; et al. A peptide that binds and stabilizes p53 core domain: chaperone strategy for rescue of oncogenic mutants. *Proc. Natl. Acad. Sci. U.S.A.* **2002**, *99*, 937−942.

(14) Domenici, F.; Frasconi, M.; Mazzei, F.; D'Orazi, G.; Bizzarri, A. R.; Cannistraro, S. Azurin modulates the association of Mdm2 with p53: SPR evidence from interaction of the full-length proteins. *J. Mol. Recognit.* **2011**, *24*, 707−714.

(15) Funari, G.; Domenici, F.; Nardinocchi, L.; Puca, R.; D'Orazi, G.; Bizzarri, A. R.; Cannistraro, S. Interaction of p53 with Mdm2 and azurin as studied by atomic force spectroscopy. *J. Mol. Recognit.* **2010**, *23*, 343−351.

(16) Punj, V.; Das Gupta, T. K.; Chakrabarty, A. M. Bacterial cupredoxin azurin and its interactions with the tumor suppressor protein p53. *Biochem. Biophys. Res. Commun.* **2003**, *312*, 109−114.

(17) Yamada, T.; Hiraoka, Y.; Ikehata, M.; Kimbara, K.; Avner, B. S.; Das Gupta, T. K.; Chakrabarty, A. M. Apoptosis or growth arrest: Modulation of tumor suppressor p53's specificity by bacterial redox protein azurin. *Proc. Natl. Acad. Sci. U.S.A.* **2004**, *101*, 4770−4775.

(18) Yamada, T.; Goto, M.; Punj, V.; Zaborina, O.; Chen, M. L.; Kimbara, K.; Majumdar, D.; Cunningham, E.; Das Gupta, T. K.; Chakrabarty, A. M. Bacterial redox protein azurin, tumor suppressor protein p53, and regression of cancer. *Proc. Natl. Acad. Sci. U.S.A.* **2002**, *99*, 14098−14103.

(19) Lobato, C. Conditioned Medium From Azurin-Expressing Human Mesenchymal Stromal Cells Demonstrates Antitumor Activity Against Breast and Lung Cancer Cell Lines. *Front. Cell Dev. Biol.* **2020**, *8*, No. 471.

(20) Yamada, T.; Gupta, T. K. Das.; Beattie, C. W. p28-Mediated Activation of p53 in G2−M Phase of the Cell Cycle Enhances the Efficacy of DNA Damaging and Antimitotic Chemotherapy. *Cancer Res.* **2016**, *76*, 2354−2365.

(21) Bizzarri, A. R.; Moscetti, I.; Cannistraro, S. BBA - General Subjects Interaction of the anticancer p28 peptide with p53-DBD as studied by fl uorescence, FRET, docking and MD simulations. *Biochim. Biophys. Acta* **2019**, *1863*, 342−350.

(22) Yang, J.; Yan, R.; Roy, A.; Xu, D.; Poisson, J.; Zhang, Y. The I-TASSER suite: Protein structure and function prediction. *Nat. Methods* **2014**, *12*, 7−8.

(23) Duan, J.; Nilsson, L. Effect of Zn2+ on DNA recognition and stability of the p53 DNA-binding domain. *Biochemistry* **2006**, *45*, 7483−7492.

(24) Calimet, N.; Simonson, T. Cys-HisZn^2 interactions: Possibilities and limitations of a simple pairwise force field. *J. Mol. Graphics* **2006**, *24*, 404−411.

(25) De Grandis, V.; Bizzarri, A. R.; Cannistraro, S. Docking study and free energy simulation of the complex between p53 DNA-binding domain and azurin. *J. Mol. Recognition* **2007**, *20*, 215−226.

(26) Bizzarri, A. R.; Santini, S.; Coppari, E.; Bucciantini, M.; Di Agostino, S.; Yamada, T.; Beattie, C. W.; Cannistraro, S. Interaction of an anticancer peptide fragment of azurin with p53 and its isolated domains studied by atomic force spectroscopy. *Int. J. Nanomed.* **2011**, *6*, 3011−3019.

(27) Abraham, M. J.; Murtola, T.; Schulz; Roland Shultz, S. P.; Smith, J. C.; Hess, B.; Lindah, E. Gromacs: High performance molecular simulations through multi-level parallelism from laptops to supercomputers. *SoftwareX* **2015**, *1−2*, 19−25.

(28) Ponder, J. W.; Case, D. A. Force Fields for Protein Simulations. *Adv. Protein Chem.* **2003**, *66*, 27−85.

(29) Berendsen, H. J. C.; Grigera, J. R.; Straatsma, T. P. The missing term in effective pair potentials. *J. Phys. Chem. A* **1987**, *91*, 6269−6271.

(30) Santini, S.; Bizzarri, A. R.; Cannistraro, S. Modelling the interaction between the p53 DNA-binding domain and the p28 peptide fragment of Azurin. *J. Mol. Recognit.* **2011**, *24*, 1043−1055.

(31) Hess, B.; Bekker, H.; Berendsen, H. J. C.; Fraaije, J. G. E. M. LINCS: A linear constraint solver for molecular simulations. *J. Comput. Chem.* **1997**, *18*, 1463−1472.
(32) Kholmurodov, K.; Smith, W.; Yasuoka, K.; Darden, T.; Ebisuzaki, T. A smooth-particle mesh Ewald method for DL_POLY molecular dynamics simulation package on the Fujitsu VPP700. *J. Comput. Chem.* **2000**, *21*, 1187−1191.
(33) Darden, T.; York, D.; Pedersen, L. Particle mesh Ewald: An N·log(N) method for Ewald sums in large systems. *J. Chem. Phys.* **1993**, *98*, 10089−10092.
(34) Nosé, S. A unified formulation of the constant temperature molecular dynamics methods. *J. Chem. Phys.* **1984**, *81*, 511−551.
(35) Parrinello, M.; Rahman, A. Polymorphic transitions in single crystals: A new molecular dynamics method. *J. Appl. Phys.* **1981**, *52*, 7182−7190.
(36) Eisenhaber, F.; Lijnzaad, P.; Argos, P.; Sander, C.; Scharf, M.; Eisenhaber, F.; Lijnzaad, P.; Argos, P.; Sander, C.; S, M. The Double Cubic Lattice Method: Efficient Approaches to Numerical Integration of Surface Area and Volume and to Dot Surface Contouring of Molecular Assemblies. *J. Comput. Chem.* **1995**, *16*, 273−284.
(37) Guex, N.; Peitsch, M. C. SWISS-MODEL and the Swiss-PdbViewer: An environment for comparative protein modeling. *Electrophoresis* **1997**, *18*, 2714−2723.
(38) Humphrey, W. F.; Dalke, A.; Schulten, K. VMD-visual molecular dynamics. *J. Mol. Graphics* **1996**, *14*, 33−38.
(39) Amadei, A.; Linssen, A. B. M.; Berendsen, H. J. C. Essential dynamics of proteins. *Proteins Struct., Funct., Genet.* **1993**, *17*, 412−425.
(40) Amadei, A.; Linssen, A. B. M.; de Groot, B. L.; van Aalten, D. M. F.; Berendsen, H. J. C. An Efficient Method for Sampling the Essential Subspace of Proteins. *J. Biomol. Struct. Dyn.* **1996**, *13*, 615−625.
(41) de Groot, B. L.; Amadei, A.; van Aalten, D. M. F.; Berendsen, H. J. C. Towards an Exhaustive Sampling of the Configurational Spaces of the Two Forms of the Peptide Hormone Guanylin. *J. Biomol. Struct. Dyn.* **1996**, *13*, 741−751.
(42) Cho, Y. J.; Gorina, S.; Jeffrey, P. D.; Pavletich, N. P. Crystal-structure of a p53 tumor-suppressor DNA complex-understanding tumorigenic mutations. *Science* **1994**, *265*, 346−355.
(43) Signorelli, S.; Santini, S.; Yamada, T.; Bizzarri, A. R.; Beattie, C. W.; Cannistraro, S. Binding of Amphipathic Cell Penetrating Peptide p28 to Wild Type and Mutated p53 as studied by Raman, Atomic Force and Surface Plasmon Resonance spectroscopies. *Biochim. Biophys. Acta* **2017**, *1861*, 910−921.
(44) Alcala, J. R.; Gratton, E.; Prendergast, F. G. Fluorescence lifetime distributions in proteins. *Biophys. J.* **1987**, *51*, 597−604.
(45) Frauenfelder, H.; Chen, G.; Berendzen, J.; Fenimore, P. W.; Jansson, H.; McMahon, B. H.; Stroe, I. R.; Swenson, J.; Young, R. D. A unified model of protein dynamics. *Proc. Natl. Acad. Sci. U.S.A.* **2009**, *106*, 5129−5134.
(46) Frauenfelder, H.; Parak, F. P.; Young, R. D. Conformational substates in proteins. *Annu. Rev. Biophys. Biophys.Chem.* **1988**, *17*, 451−479.
(47) Bizzarri, A. R.; Paciaroni, A.; Cannistraro, S. Glasslike dynamical behavior of the plastocyanin hydration water. *Phys. Rev. E* **2000**, *62*, 3991−3999.
(48) Bizzarri, A. R.; Cannistraro, S. Molecular Dynamics of Water at the Protein - Solvent Interface. *J. Phys. Chem. B* **2002**, *106*, 6617−6633.
(49) Lee, K. C. B.; Siegel, J.; Webb, S. E. D.; Lévêque-Fort, S.; Cole, M. J.; Jones, R.; Dowling, K.; Lever, M. J.; French, P. M. W. Application of the stretched exponential function to fluorescence lifetime imaging. *Biophys. J.* **2001**, *81*, 1265−1274.
(50) Lakowicz, J. R. *Principles of Fluorescence Spectroscopy*, 3rd ed.; Springer, 2006.
(51) Sugio, S.; Kashima, A.; Mochizuki, S.; Noda, M.; Kobayashi, K. Crystal structure of human serum albumin at 2.5 Å resolution. *Protein Eng., Des. Sel.* **1999**, *12*, 439−446.
(52) Yuqin, L.; Guirong, Y.; Zhen, Y.; Caihong, L.; Baoxiu, J.; Jiao, C.; Yurong, G. Investigation of the interaction between patulin and human serum albumin by a spectroscopic method, atomic force microscopy, and molecular modeling. *Biomed. Res. Int.* **2014**, *2014*, No. 734850.
(53) Santini, S.; Bizzarri, A. R.; Cannistraro, S. Revisitation of FRET methods to measure intraprotein distances in Human Serum Albumin. *J. Lumin.* **2016**, *179*, 322−327.
(54) Chen, Y.; Barkley, M. D. Toward Understanding Tryptophan Fluorescence in Proteins. *Biochemistry* **1998**, *37*, 9976−9982.

https://dx.doi.org/10.1021/acs.jpcb.0c06778
J. Phys. Chem. B XXXX, XXX, XXX−XXX